



**HAL**  
open science

# Influence of ionic interactions on lithium diffusion properties in ionic liquid-based gel polymer electrolytes

H. Porthault, G. Piana, J.M. Duffault, S. Franger

## ► To cite this version:

H. Porthault, G. Piana, J.M. Duffault, S. Franger. Influence of ionic interactions on lithium diffusion properties in ionic liquid-based gel polymer electrolytes. *Electrochimica Acta*, 2020, 354, pp.136632 -. 10.1016/j.electacta.2020.136632 . hal-03490171

**HAL Id: hal-03490171**

**<https://hal.science/hal-03490171>**

Submitted on 28 Jun 2022

**HAL** is a multi-disciplinary open access archive for the deposit and dissemination of scientific research documents, whether they are published or not. The documents may come from teaching and research institutions in France or abroad, or from public or private research centers.

L'archive ouverte pluridisciplinaire **HAL**, est destinée au dépôt et à la diffusion de documents scientifiques de niveau recherche, publiés ou non, émanant des établissements d'enseignement et de recherche français ou étrangers, des laboratoires publics ou privés.



Distributed under a Creative Commons Attribution - NonCommercial 4.0 International License

# Influence of Ionic Interactions on Lithium Diffusion Properties in Ionic Liquid-Based Gel Polymer Electrolytes

H. Porthault<sup>a</sup>, G. Piana<sup>a,b</sup>, J.M. Duffault<sup>b</sup>, S. Franger<sup>b</sup>

<sup>a</sup> *Univ. Grenoble Alpes, CEA, LETI, MINATEC Campus, 38054 Grenoble, France*

<sup>b</sup> *Univ. Paris Sud / Univ. Paris-Saclay, Institut de Chimie Moléculaire et des Matériaux d'Orsay  
(UMR CNRS 8182), Orsay, France*

*\*corresponding author: H. Porthault*

## Abstract

In this study, we characterize a ternary gel polymer electrolyte (GPE) composed of bisphenol A ethoxylate dimethacrylate (BEMA) and N-propyl-N-methylpyrrolidinium bis(trifluoromethanesulfonyl)imide (PYR<sub>13</sub>TFSI) ionic liquid and we particularly study the influence of salt content and polymer network composition. The effect of salt concentration in liquid solutions (1-x)PYR<sub>13</sub>TFSI-xLiTFSI (molar ratio  $R = x/(1-x)$ ) is finely characterized by Arrhenius measurements, PFG-NMR and Raman spectroscopy. They highlight ions interactions evolution with the salt content. For lower salt concentrations, ions pairs with bidentate coordinations  $[\text{Li}(\text{TFSI})_2]^-$  are preferentially formed. A salt content rise leads to the formation of ionic aggregates where several  $\text{Li}^+$  are bound by  $\text{TFSI}^-$  to form  $[\text{Li}_z(\text{TFSI})_y]^{(z-y)}$  large clusters. These ionic arrangements changes modify the mean charge of the complexes involving Li. It leads to better cycling performances with higher salt concentration contrary to the ionic conductivity evolution. When the binary solution is added to the GPE, a dual transport mechanism, by diffusion in the liquid phase and hops assisted by segmental

motion, is confirmed. The Li transference number is improved with success by enhancing this segmental motion with the addition of a linear polymer (poly(ethylene glycol) methyl ether methacrylate, me-PEGMA). Cycling with 70 % of theoretical capacity and improved high current ability is achievable at 25°C with a dual me-PEGMA/BEMA polymer network.

## **Keywords**

Lithium metal batteries, Gel polymer electrolytes, photo-initiated reticulation, ionic liquids, lithium transport.

## **Introduction**

The internet of things (IOT) is experiencing a huge development since the 2000s. New objects emerged in everyday life applications like wearables for healthcare or fashion (medical ships, functionalized clothing, etc.) and securing of personal data (secured smart cards, etc.). These applications require new needs like high temperature ability to be compatible with smart cards selling process, flexibility to be mechanically compliant for wearables applications, limited thickness (< 500 μm) to be easily integrated etc. However, the main aspect remains the safety from a physiological aspect for healthcare applications (low toxicity, bio-compatibility, etc.) and a physicochemical feature (low flammability, no leakage concerns, etc.) [1-3]. Many studies are then carried out to substitute the classical liquid electrolyte with a solid one. Considering the flexibility and mechanical requirements of these new applications, solid polymer electrolytes (SPE) [4] or ceramic electrolytes [5] cannot be considered. Gel polymer electrolytes (GPE), where a solvent and/or a liquid plasticizer is incorporated into the polymer network-salt system, turns out to be a good alternative material [6-9]. This concept is developed from the 1975 by Feuillade *et al* [10]

and applications in lithium ion batteries are reported since the 1990s by Tarascon *et al* [11] with solid polymer matrixes encompassing solution of carbonates (EC:DMC) and  $\text{LiPF}_6$  salt. The use of unstable liquids reduces the safety beside the SPE. Hence, since the 2000s, many teams added ionic liquids as solvent due to their high thermal stability and low vapor pressure [12-14]. Main ionic liquids reported in the literature as electrolytes are initially based on imidazolium cations because of their high conductivity and low viscosity. Nevertheless, quaternary ammonium, like pyrrolidinium or piperidinium, are now widely used due to their higher electrochemical stability and compatibility with Li metal anodes [15]. Furthermore, in addition to the smart choice of the ionic liquid, the lithium salt also has a main influence on the battery performance as it insures the lithium ionic conductivity. The almost exclusively salt used in commercial Li-ion batteries is the lithium hexafluorophosphate  $\text{LiPF}_6$  that exhibits high ionic conductivity, good electrochemical stability and prevents the corrosion of the aluminum current collector. However, its high moisture sensitivity (forming HF) and low thermal stability ( $< 55\text{ }^\circ\text{C}$ ) make it not consistent with new applications. More promising salts are currently developed to substitute  $\text{LiPF}_6$  and among them, lithium bis(trifluoromethanesulfonyl)imide  $\text{LiTFSI}$  and lithium bis(florosulfonyl)imide  $\text{LiFSI}$  seem to be the best candidates.  $\text{TFSI}^-$  anion is chosen in this study regarding its better thermal stability despite its lower conductivity [15]. Nevertheless, salt concentration also greatly influences performances. Hence, even if low salt concentrations are considered favorable for many years (higher conductivity at low temperature related to lower viscosity) [16, 17], increasing number of studies report positive impact of higher salt concentration [18], going up to "superconcentrated electrolyte" [19], namely concentrations higher than  $3\text{ mol L}^{-1}$ . The choice of the polymer matrix containing the liquid solution is also essential. In many works, GPE is formed by solvent evaporation.

The polymer chains (typically linear PEO or PVDF compounds) are linked by weak Van der Waals and hydrogen bonds [6]. It results in low mechanical properties particularly for samples with high liquid proportion. On the other hand, a crosslinked host polymer creates a chemical gel with the formation of strong covalent bonds. It leads to higher mechanical properties and better liquid retention [20]. Crosslinking can be achieved by thermal curing [21, 22] or photo-initiated processes [23-29]. The structure of the polymer network plays an important role on the electrochemical performances and some groups tune the transport properties by mixing different polymers for example by adding pending linear chains [30].

In a previous work [31], we have already reported on the influence of the UV-curing on the electrochemical properties. In the present work, we focus on the effect of the salt concentration, mainly in high concentration range ( $\geq 1 \text{ mol L}^{-1}$ ), and the polymer network composition on the GPE properties. A special interest is dedicated to the influence of ionic interactions in the binary solution (lithium salt and ionic liquid) and between the liquid phase and the polymer network. This results in an optimization strategy by linear polymer addition.

## **1. Experimental**

### *1.1. Materials and samples preparation*

Bisphenol A ethoxylate dimethacrylate (BEMA,  $M_n \sim 1700$ , EO/phenol 15), Darocur<sup>®</sup> 1173 (97 %), poly(ethylene glycol) methyl ether methacrylate (me-PEGMA,  $M_n \sim 500$ ), and bis(trifluoromethane)sulfonimide lithium salt (LiTFSI, 99.95 %) are purchased from Sigma Aldrich. N-propyl-N-methylpyrrolidinium bis(trifluoromethanesulfonyl)imide (PYR<sub>13</sub>TFSI, 99.9 %) is purchased from Solvionic (Figure 1).

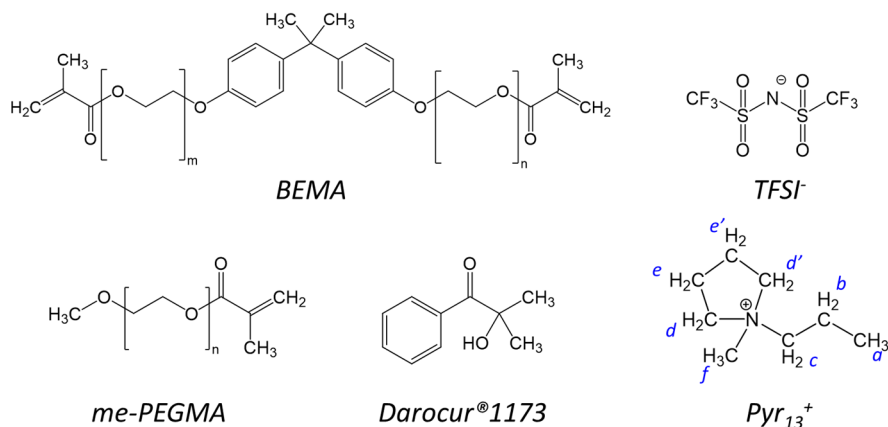


Figure 1: Chemical Structures of BEMA and me-PEGMA host polymer, Darocur1173 photo-initiator, Pyr<sub>13</sub><sup>+</sup> cation (with <sup>1</sup>H NMR assignments) and LiTFSI salt.

The binary solution composing the GPE is defined as (1-x) Pyr<sub>13</sub>TFSI : x LiTFSI where x is the molar content of LiTFSI and R, the molar ratio, is defined in eq.1. The corresponding values in mol L<sup>-1</sup> are given in supporting file, Table S1.

$$R = \frac{x}{1-x} \quad (\text{eq.1})$$

The GPE electrolyte is composed of this binary liquid solution with various R and BEMA as host polymer in an initial 70:30 wt % ratio. The synthesis procedure is the same than the one described in our previous study [31] and is reminded in the supporting file. The influence of the UV-curing parameters being described previously [31], the curing conditions are fixed here at 3 min at 3 mW cm<sup>-2</sup>. Depending on the characterization, GPE membrane can be self-standing or directly realized on a substrate as shown in Figure 2a and b.

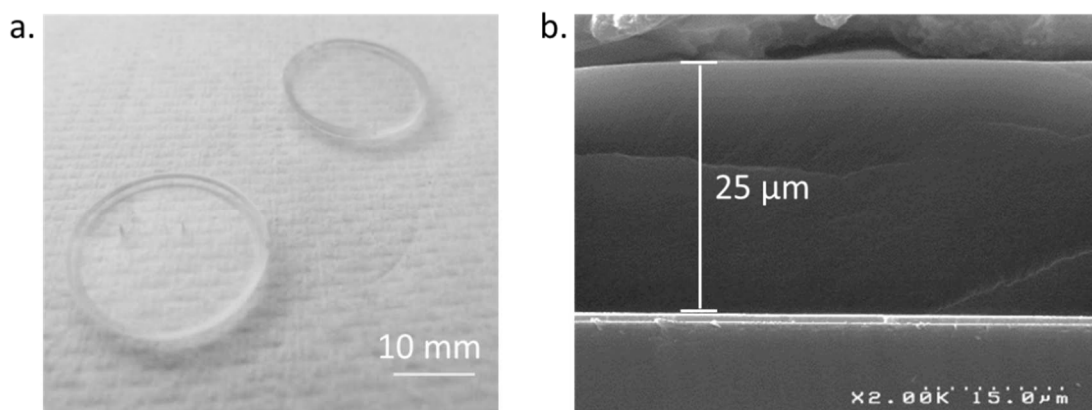


Figure 2: Optical view of self-standing GPE membranes (a) and SEM cross section view of a GPE directly deposited and cured on a substrate (b).

## 2.2 Characterizations

Thermogravimetric (TGA) and Differential Scanning Calorimetric (DSC) analyses are carried out using a Q500 Model (TA Instruments). For TGA, samples are heated at  $5\text{ }^{\circ}\text{C min}^{-1}$  up to  $600\text{ }^{\circ}\text{C}$  under argon atmosphere. For DSC analyses, samples are at first cooled down to  $-40\text{ }^{\circ}\text{C}$  and then heated up to  $150\text{ }^{\circ}\text{C}$  at  $10\text{ }^{\circ}\text{C min}^{-1}$  under nitrogen atmosphere.

Mechanical properties are determined using Dynamic Mechanical Analysis (DMA) under shearing (Dynatest Metravib VA 2000 instrument) as previously described [31] and reminded in supporting file. Measurements are carried out with a dynamic displacement of  $5\text{ }\mu\text{m}$  at  $0.1\text{ Hz}$  frequency between  $-120\text{ }^{\circ}\text{C}$  and  $150\text{ }^{\circ}\text{C}$  with a temperature control of  $2\text{ }^{\circ}\text{C min}^{-1}$ .

Viscosity determination is done under shearing stress using a Bohlin CVO rheometer (Malvern) with a plan-cone configuration. Values are determined at  $25\text{ }^{\circ}\text{C}$  with a shearing rate of  $100\text{ s}^{-1}$  ( $150\text{ }\mu\text{m}$  gap).

Electrochemical Impedance Spectroscopy (EIS) is used to determine ionic conductivity (Biologic VMP3,  $100\text{ mHz}$ - $1\text{ MHz}$ ,  $10\text{ mV}$ ) in a symmetric Pt-Pt Biologic HTCC-conductivity cell ( $k = 1.0\text{ cm}^{-1}$ ) for both liquid binary solutions and GPE. For the GPE study, the liquid

precursors solution is put in the conductivity cell glass vial, electrodes are dipped into the solution and the cell is closed under argon atmosphere. The solution is then directly UV-polymerized through the glass. The electrolyte resistance is considered to be the high frequency one, assuming that the connection resistances are negligible. Arrhenius measurements are then carried out between 25 and 80 °C (298-353 K).

Considering the high ionic liquid content media, the most popular Bruce & Vincent or Watanabe electrochemical techniques [32-35] to determine the Li transference number, where the assumptions are for dilute solutions, are hardly applicable. Therefore, in this work, as it was done in our previous study, we chose to evaluate the transference number by PFG-NMR technique from the diffusion coefficients determination ([31, 36], supporting file). As a reminder, this technique takes into account all mobile species, including those that do not contribute to the current transport, leading to a slight overestimation of the  $T_{Li}$  value.

Raman spectroscopy is carried out using a Renishaw inVia equipment with a 785 nm laser in the 200-1800  $\text{cm}^{-1}$  range. For binary solutions, spectra are normalized in regards to the 1240  $\text{cm}^{-1}$  peak assigned to the TFSI<sup>-</sup> -CF<sub>3</sub> group which is not affected by ionic interactions [37]. The focus is then done on the 700-800  $\text{cm}^{-1}$  area.

Cycling performance are evaluated using CR2032 coin cells sealed under argon. To avoid limitation by the electrode (porosity soaking, composition influence, etc.), we chose to work on a "model" electrode material. Currently, there is many various cathodic materials, mainly intercalation ones like LiCoO<sub>2</sub> or the high voltage LiNi<sub>x</sub>Mn<sub>y</sub>Co<sub>z</sub>O<sub>2</sub> group [3, 38]. In this paper, we choose to test our GPE with the well-known LiCoO<sub>2</sub> cathodic material. The positive electrode is thus a pure LiCoO<sub>2</sub> material deposited by sputtering process on titanium foil

substrate. The deposit thickness is about 1  $\mu\text{m}$  and the material is thermally treated for 2h at 600°C to obtain the desired *R-3m* phase [39]. 16 mm diameter discs are then cut to obtain cathodes ( $S = 2.01 \text{ cm}^2$ ). The capacity observed with standard liquid electrolyte (EC:PC:DMC 1:1:3 1 M  $\text{LiPF}_6$ ) is 65.6  $\mu\text{Ah cm}^{-2}$  or 130  $\text{mAh g}^{-1}$ . 16.5 mm discs of Whatman GF/A are used as glass fiber separator for tests with liquid binary solution. For cycling with gel polymer electrolyte, a Celgard 2400 ring (14 mm internal diameter) is used as shim (18  $\mu\text{m}$  thickness) instead of the Whatman separator, the active surface is then 1.54  $\text{cm}^2$ . 20  $\mu\text{L}$  of liquid GPE precursor solution are deposited on the cathode material by drop casting and directly cured by UV-irradiation process. The system is then put into the CR2032 coin cell with Li metal foil (Albemarle, 135  $\mu\text{m}$ ) as anode. The electrochemical stability window of a GPE with a molar ratio R of 0.3 is 1.5-4.25V vs  $\text{Li}^+/\text{Li}$  considering a degradation current density lower than 2  $\mu\text{A cm}^{-2}$  (Supporting file, Figure S2). This anodic stability enable the galvanostatic cycling between 3.0 and 4.2 V vs  $\text{Li}^+/\text{Li}$  done at 25 °C under various current (from 15 to 60  $\mu\text{A}$ ).

## 2. Results and Discussion

### 3.1 Influence of the salt content in liquid binary solutions

DSC thermograms (Supporting file Figure S3) of the neat Pyr<sub>13</sub>TFSI exhibits an endothermic melting peak at 13.30 °C, close to the value reported in the literature (10 °C [40]). When the Li salt is added, two endothermic peaks appear at 3.47 °C and 18.79 °C showing two distinct transitions characteristic of a solid solution. This result is consistent with the phase diagram of the LiTFSI-Pyr<sub>13</sub>TFSI system reported in the literature [41]. According to this phase diagram, this solid solution is liquid at 25 °C up to  $x = 0.33$  ( $R=0.5$ ). However, the solution is visually still liquid up to  $x = 0.375$  ( $R = 0.6$ ) at 25 °C and becomes solid around 20 °C. This concentration is then considered in this study as the maximum quantity of salt dissolved in the ionic liquid.

The solution viscosity (Figure 3a) increases exponentially with the salt content. As expected, the ionic conductivity at 25 °C (Figure 3a) decreases with salt content inversely to the viscosity, from 4.12 to 0.25 mS cm<sup>-1</sup> for  $R = 0$  and 0.6 respectively. The Walden plot (Figure 3b) exhibits a linear evolution of  $\log \Lambda_m$  (the molar conductivity in S cm<sup>2</sup> mol<sup>-1</sup>) vs  $\log (1/\eta)$  (the viscosity in P). The curve is slightly below the ideal one obtained with a liquid KCl solution (black line). MacFarlane *et al* [42] reported the same tendency for the neat ionic liquid (Pyr<sub>13</sub>TFSI, pink line reported in the insert). This deviation from the Walden rule ( $\Lambda_m\eta = \text{constant}$ ) is attributed to ionic associations, mainly the strong Li<sup>+</sup>-TFSI<sup>-</sup> interactions occurring in this system as previously reported by Giffin *et al* [43]. This leads to an increase of the solution viscosity and its glass transition temperature. The Arrhenius plots of these compositions are shown in Figure 3c. The ionic conductivity increases with temperature due to the viscosity decrease. Measurements cannot be done below 25 °C for  $R = 0.6$  due to the

liquid to solid-like conversion of the system leading to a very high resistance. For the R = 0.3 solution, a slope discontinuity is observed between 15 °C and 20 °C also due to the liquid to solid transition as observed in DSC thermograms with a melting temperature of 18.8 °C. Above these transition temperatures, the evolution of the conductivity curves can be fitted by the Vogel-Tammann-Fulcher (VTF) equation [44, 45] with good correlation parameters ( $R^2 > 0.999$ ) (Table 1):

$$\sigma = \frac{A}{\sqrt{T}} \cdot \exp\left(\frac{-B}{k_B(T-T_0)}\right) \quad (\text{eq.2})$$

With A ( $\text{S cm}^{-1} \text{K}^{-1/2}$ ) a pre-factor correlated to the charge carriers numbers, B (J) the pseudo-activation energy,  $T_0$  (K) the theoretical glass transition temperature  $T_g$  and  $k_B$  the Boltzmann constant ( $1.3806 \text{ J K}^{-1}$ ). Used for ionic liquids or polymer electrolytes, this model assume that species motion is governed by the free volume redistribution and not the thermal activation. The temperature rise leads to the material expansion and the free volume increase. The B constant is called "pseudo-activation energy" since it is not really related to an activation mechanism but depends on the species motion resulting from the free volume ordering. This parameter is inversely proportional to the liquid fragility index  $m$ , directly related to the ionic conductivity and depending on the liquid ionicity and the anion size. Sippel *et al* [46] showed that highest ionic conductivities are achieved by liquids combining low glass temperature and high fragility index, thus low pseudo-activation energy B. This B parameter is low for studied solutions (Table 1) and values are close to the toluene one ( $1/m \sim 5.6$  [47]) which means that solutions can be considered as a fragile material. B parameter increases with salt content meaning that required energy for species motion rises, which is in good accordance with the viscosity evolution. In this VTF model, the theoretical glass transition temperature  $T_0$  represents an ideal temperature from which polymer chains of the system start to be

mobile. This  $T_0$  is systematically lower than the glass transition temperature  $T_g$  and the approximation  $T_0 = T_g - 50$  K is usually used [48, 49]. This  $T_0$  parameter increases with molar ratios  $R$  meaning that species are less mobile. For  $R = 0$ , the calculated  $T_g^*$  temperature is -53.6 °C. This value is hard to compare to the literature considering that besides MacFarlane *et al.* [50] who reported a  $T_g$  of about -90 °C, most of other groups [51, 52] do not detect any glass transition for the neat Pyr<sub>13</sub>TFSI. However, the reported experimental  $T_g$  values for others alkyl pyrrolidinium chains [52, 53] seems to be lower than  $T_g^*$  calculated in our study but its evolution (increase with salt content) is the same [54]. When the lithium salt is added, the  $A$  parameter, referring to charge carriers number, slightly decreases with salt molar ratio. This decrease is attributed to the viscosity increase and is probably amplified by the formation of neutral ion pair associations or ionic complex  $[\text{Li}(\text{TFSI})_{n+1}]^{n-}$  limiting the number of charge carriers [48, 54].

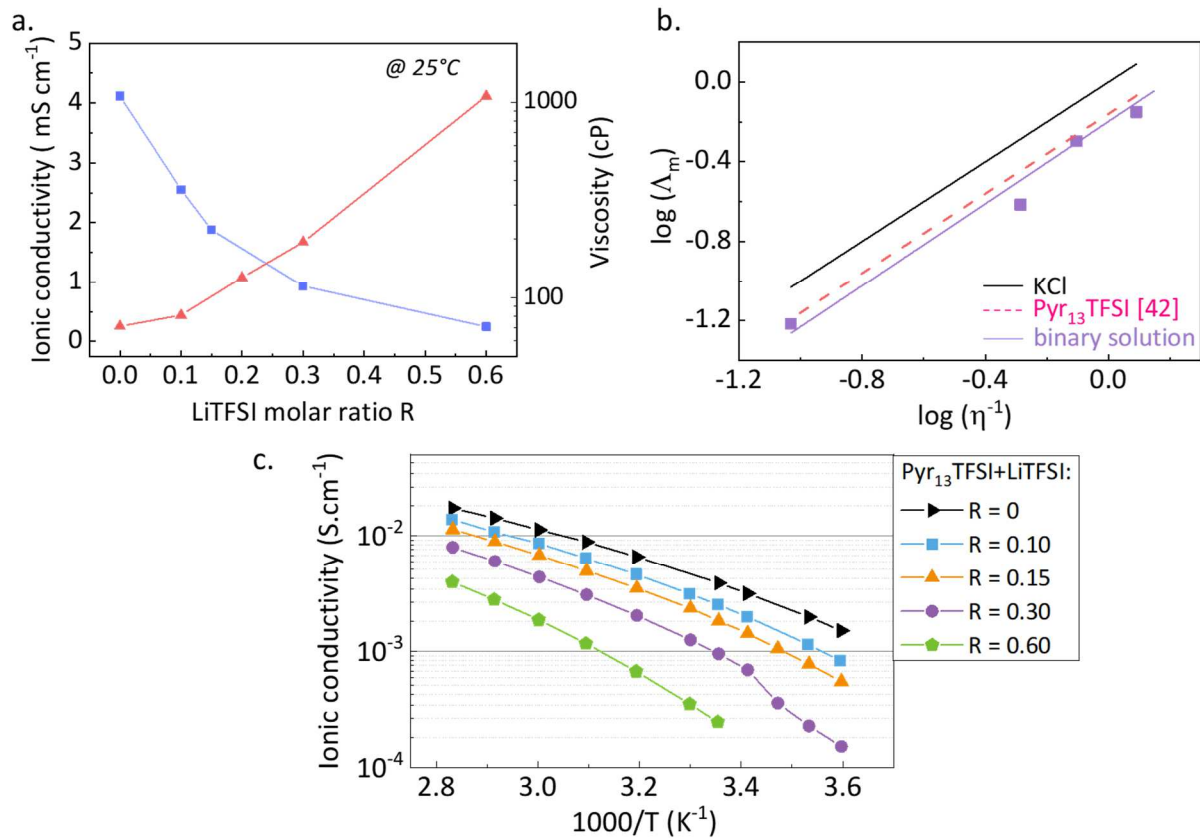


Figure 3: Ionic conductivity and viscosity measurements at 25 °C for various LiTFSI molar ratios (a), Walden plot (Pyr<sub>13</sub>TFSI reported from [42]) (b) and associated Arrhenius plots (c).

LiTFSI Molar Ratio R	$\sigma_{25^\circ\text{C}}$ $\text{mS cm}^{-1}$	VTF parameters					$T_g^*=T_0+50$ $^\circ\text{C}$
		A	B		$T_0$		
		$\text{S cm}^{-1} \text{K}^{1/2}$	eV	$\text{kJ mol}^{-1}$	K	$^\circ\text{C}$	
0	4.12	12.98	0.058	5.62	169.6	-103.6	-53.6
0.10	2.55	18.91	0.059	5.69	165.6	-107.6	-57.6
0.15	1.88	17.73	0.070	6.74	169.8	-103.4	-53.4
0.30	0.93	17.34	0.071	6.86	179.5	-93.7	-43.7
0.60	0.25	16.63	0.074	7.11	195.9	-77.3	-27.3

*Table 1: Ionic conductivity at 25°C, VTF fitting parameters and theoretical glass transition temperature  $T_g^*$  extrapolated from  $T_0$  values for each R molar ratio solution.*

To elucidate the contribution of each ion to the global conductivity, NMR spectroscopy is conducted on the three nuclei  $^1\text{H}$ ,  $^7\text{Li}$  and  $^{19}\text{F}$ . The salt molar ratio increase induces a peaks broadening on NMR spectra (not shown here) reflecting the restriction of molecules mobility which is consistent with viscosity increase. Likewise, all diffusion coefficients of each nucleus, measured by PFG-NMR spectroscopy and reported in Figure 3a, decrease with salt content. In all tested samples, the  $\text{Pyr}_{13}$  molecules diffuse faster than TFSI and Li is consistently slower than both of them:  $D_{\text{Pyr}_{13}} > D_{\text{TFSI}} \gg D_{\text{Li}}$ . This result is in good accordance with the literature [41, 55] but not consistent with the Stokes-Einstein diffusion law prescribing that smaller particles diffuse faster. As NMR technique detects the nucleus signal, there is no distinction between ions and neutral species. Therefore, measured diffusion coefficients represent an average value of ions and its complexes. This low diffusion coefficient of lithium can then be attributed to the strong interactions with TFSI<sup>-</sup> anions creating large

$[\text{Li}(\text{TFSI})_{n+1}]^{n-}$  complexes as previously suggested by VTF results. The Li transference number (inset Figure 4a) increases with LiTFSI molar ratio while  $T_H$  and  $T_F$  slowly decrease. The  $T_{Li}$  transference number and the total ionic conductivity allow the determination of the apparent lithium conductivity (Figure 4b), that gives an approximation of the current fraction that would be transported by lithium species under an electrical field. Consequently, it is possible to calculate an apparent lithium conductivity, slightly overestimated as it takes into account ionic complexes and neutral species. Interestingly, the lithium conductivity exhibits a bell shape evolution with a maximum around  $R = 0.25$ . Beyond this salt content, the viscosity increase becomes the limiting phenomenon and lithium species are less mobile. A theoretical conductivity can be calculated through the Nernst-Einstein equation assuming that ion activity is equal to 1 without ionic associations (eq.3). For each ion, the charge is equal to 1 ( $\text{Pyr}_{13}^{+1}$ ,  $\text{TFSI}^{-1}$  and  $\text{Li}^{+1}$ ), the conductivity can then be expressed as follows:

$$\sigma_i = \frac{F^2}{RT} D_i c_i z_i^2 \quad (\text{eq.3})$$

$$\sigma_{NMR} = \sum \sigma_i = \frac{F^2}{RT} (D_{Pyr} c_{Pyr} + D_{TFSI} c_{TFSI} + D_{Li} c_{Li}) \quad (\text{eq.4})$$

As previously stated, the calculated conductivity (eq.4, Figure 4c), taking into account all species, is always higher than the experimental one and therefore, it is possible to define a degree of ionic association, estimating the neutral species ratio:

$$\Delta_{NMR} = 1 - \frac{\sigma_{exp}}{\sigma_{NMR}} \quad (\text{eq.5})$$

For the neat  $\text{PYR}_{13}\text{TFSI}$ , the association degree is 24 %, which means that 76 % of ions are dissociated (Figure 4c). When the molar ratio increases (up to 0.25), the association degree slightly decreases indicating that Li—TFSI interactions are stronger than  $\text{PYR}_{13}$ —TFSI ones.

When the salt content is higher, the presence of neutral complexes rises. This trend is in good accordance with results reported by Nicotera *et al* [41].

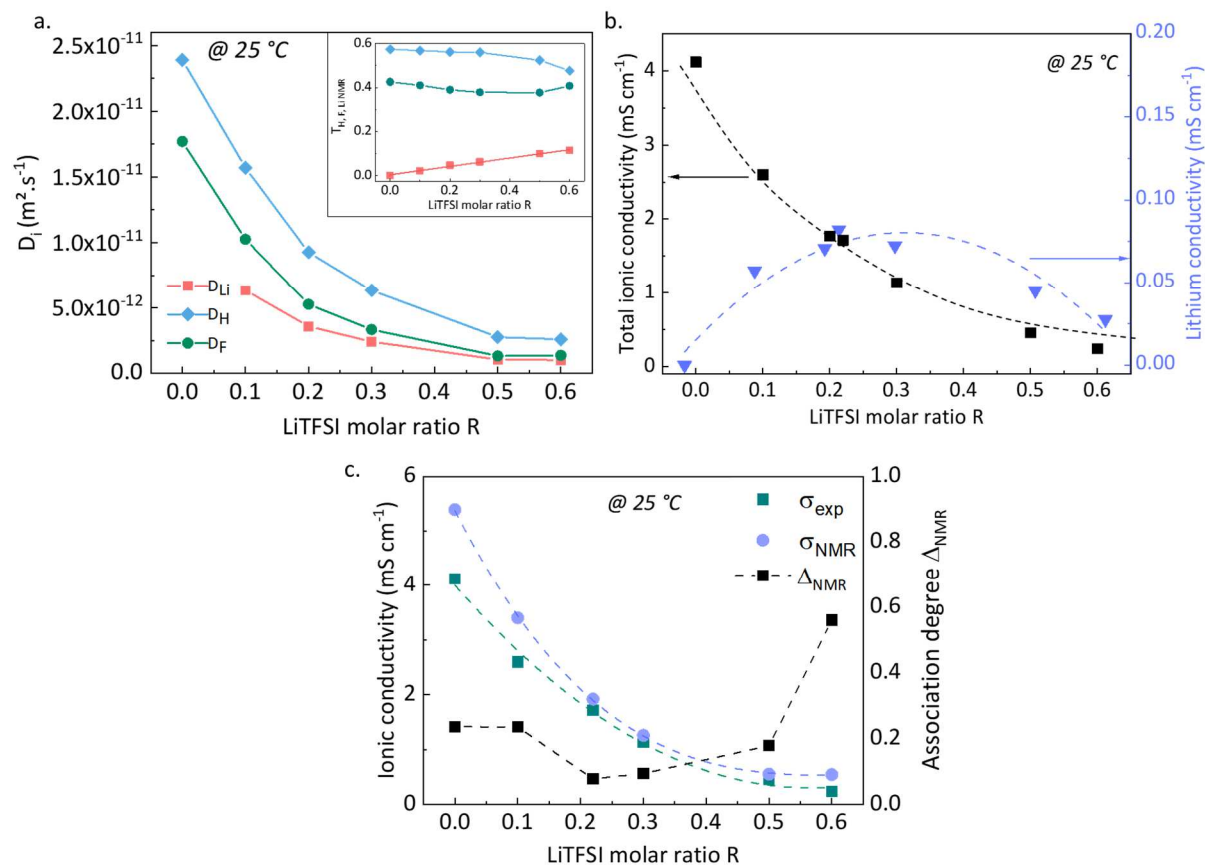


Figure 4: NMR diffusion coefficients of each nuclei for various binary solutions with the associated transference numbers (inset) (a); evolution of the total and lithium ionic conductivity for various LiTFSI molar ratios (b), evolution of the experimental and NMR calculated ionic conductivities and derived association degree for various R molar salt ratios at 25 °C (c) (dash lines for eye guidance only).

The interactions between TFSI<sup>-</sup> and Li<sup>+</sup> can be deeper characterized by Raman spectroscopy [56]. All spectrum are normalized in regards to the peak of the —CF<sub>3</sub> vibrational stretching mode around 1240 cm<sup>-1</sup> which is not modified by ionic interactions [37]. The more intense Raman signal is localized in the 800-700 cm<sup>-1</sup> range due to the overall TFSI<sup>-</sup> expansion-contraction. It is then usually studied to investigate the lithium solvation in ionic liquid. TFSI<sup>-</sup> anion presents two conformers (C<sub>1</sub> cisoid *cis* and C<sub>2</sub> transoid *trans*) but the high conformational flexibility leads to a small energy barrier (< 3.5 kJ mol<sup>-1</sup>) [57, 58] only detectable in the gas

state (peak splitting  $< 3 \text{ cm}^{-1}$ ). In the liquid state, this conformal effect only leads to the broadening of the most intense peak at  $740\text{-}742 \text{ cm}^{-1}$ , sum of  $C_1$  and  $C_2$  contributions [59]. Moreover, the negative charge of  $\text{TFSI}^-$  is highly delocalized leading to a weak coordination ability with  $\text{Pyr}_{13}^+$  cation [57] already noticed with NMR spectroscopy. Hence, both dissociated and poorly coordinated  $\text{TFSI}^-$  refers thereafter to “free”  $\text{TFSI}^-$  and are evidenced by the Raman peak around  $741 \text{ cm}^{-1}$  visible in the neat ionic liquid signal ( $R = 0$ , Figure 5a). When the molar salt content increases, this peak intensity decreases and slightly drifts towards  $743 \text{ cm}^{-1}$  with the gradual appearance of a new mode around  $748 \text{ cm}^{-1}$ . This new mode, referring to the “coordinated”  $\text{TFSI}^-$ , evidences the restrained expansion-contraction of anions coordinated with  $\text{Li}^+$ . They are coordinated in tetrahedral geometry by four oxygen of the  $-\text{SO}_2$  groups of  $\text{TFSI}^-$  molecules [60-62]. Raman spectra can then be convoluted with two functions (mix of Gaussian and Lorentzian) centered on  $741$  and  $748 \text{ cm}^{-1}$  corresponding to the “free” and “coordinated”  $\text{TFSI}^-$  anions respectively (fit example for  $R = 0.6$  in Figure 5a). The integration of fitted peaks allows to calculate the fractions of “free” and “coordinated”  $\text{TFSI}^-$  (Figure 5b). In the neat ionic liquid, the association degree  $\Delta_{\text{NMR}}$  previously determined is about 24 % whereas less than 3 % are coordinated in Raman results. This difference is attributed to the weak interactions between  $\text{TFSI}^-$  and  $\text{PYR}_{13}^+$ , neglected in Raman calculations (hardly discriminating) and taking into account as neutral  $\text{Pyr}_{13}\text{TFSI}$  species in the NMR association degree calculation. In binary solutions, when the salt content increases, the “free”  $\text{TFSI}^-$  ratio decreases for the benefit of the “coordinated”  $\text{TFSI}^-$ . A mean coordination number  $n$  can then be calculated describing the average number of  $\text{TFSI}^-$  molecules coordinated with  $\text{Li}^+$  cations. For the very low salt ratios ( $R < 0.1$ ),  $n > 2$  which means that Li are mainly part of anionic complexes with monodentates coordinations  $[\text{Li}(\text{TFSI})_4]^{3-}$ , each  $\text{TFSI}^-$  providing one oxygen atom. When the molar ratio  $R$  increases, the

mean coordination number  $n$  decreases due to the rise of bidentates complexes  $[\text{Li}(\text{TFSI})_2]^-$  where each  $\text{TFSI}^-$  provided two oxygen atoms. Above a critical molar ratio of 0.25,  $n$  seems to slightly rise again. This could be explained by the formation of aggregates network  $[\text{Li}_2(\text{TFSI})_y]^{(z-y)}$  where each Li shares several  $\text{TFSI}^-$  with its Li neighbors though the  $\text{O}=\text{S}=\text{O}$  groups. These aggregates are reported to occur when the  $\text{Li}\cdots\text{Li}$  distances are less than  $5\text{\AA}$  [59, 63].

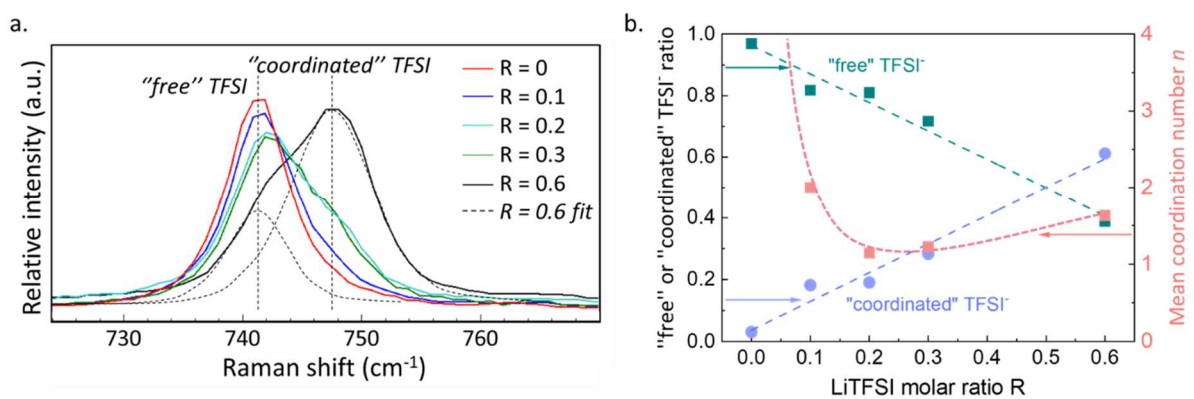


Figure 5: Raman spectra of various salt content solutions in the  $770\text{--}725\text{ cm}^{-1}$  range (a); coordinated or free  $\text{TFSI}^-$  ratios and associated mean coordination numbers of various salt contents (pink dot lines for eye guidance only) (b).

The modification of ionic arrangements is clearly evidenced in battery cycling results (Figure 6). Galvanostatic curve of mean salt content ( $R = 0.3$ , Figure 6a) at low current ( $15\ \mu\text{A}$ ) exhibits an initial polarization higher than those with standard electrolyte which leads to a lower initial discharge capacity ( $39\ \mu\text{Ah cm}^{-2}$  ie 60 % of the capacity obtained with standard liquid electrolyte). Cycling ability is improved when salt content increase, with few improvements beyond  $R = 0.4$ . The high current ability (Figure 6c) is clearly improved for the higher salt content ( $R = 0.6$ ). These results are consistent with previous assumptions established from NMR and Raman spectroscopy. For the lower salt contents ( $R < 0.2$ ), the mean coordination number ( $1 < n < 3$ ) corresponds to complex charges between 0 and -2.

Above this concentration ( $R > 0.2$ ), the total complex charge varies between 0 and  $-0.25$ . The absolute value is then lower which means that higher salt content are beneficial under an electric field. This trend is accentuated for higher currents that is clearly seen in Figure 6c. Wang *et al* [64] observed the same trends and conclude to a reinforced 3D network of  $\text{Li}^+$  coordinated with anions ( $\text{FSA}^-$  in their study) whereas bidentate complexes and free solvent divide the solution in small size areas with the lower concentration. In all cases, it demonstrates that a lower ionic conductivity does not necessarily degrades the electrochemical performances and the rate capability.

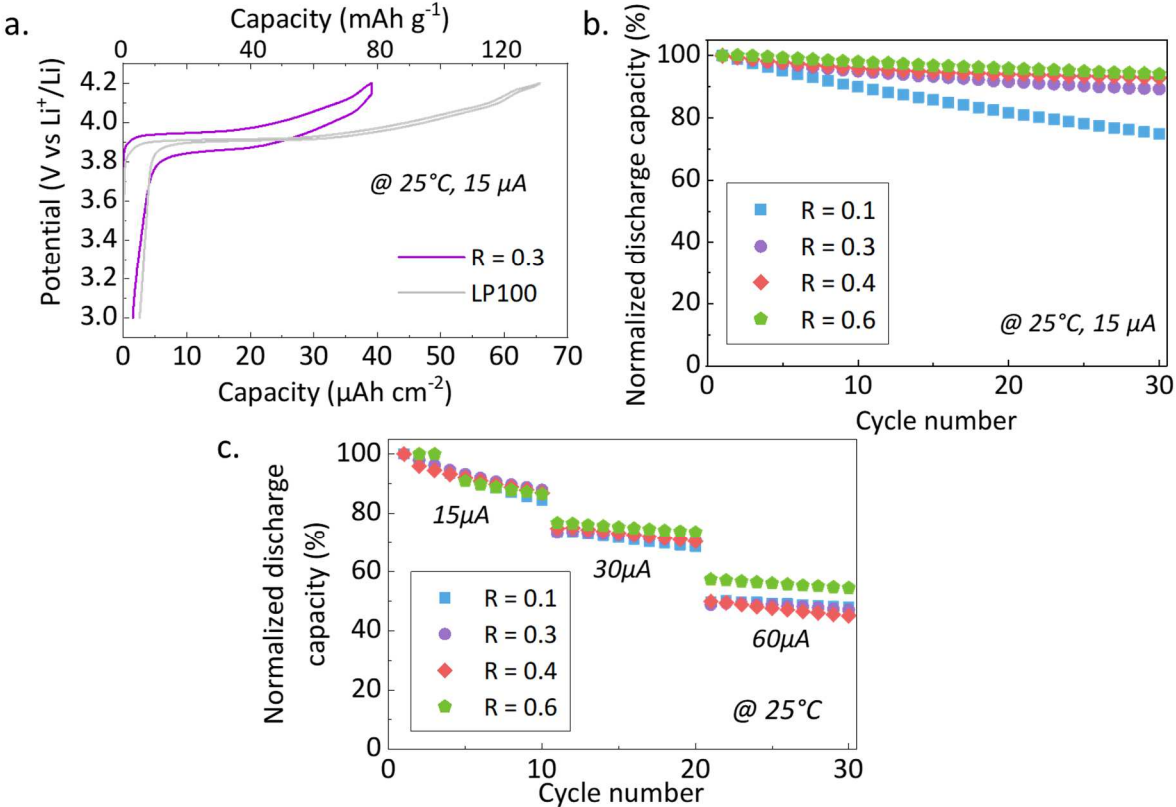


Figure 6: Galvanostatic curves for  $R = 0.3$  and standard carbonates electrolyte LP100 at  $15 \mu\text{A}$ ,  $25^\circ\text{C}$  (a), Galvanostatic cycling at  $25^\circ\text{C}$  for various salt contents: at constant current ( $15 \mu\text{A}$ ) (b), and for various currents, 10 cycles of each current (c).

### 3.2 Influence of the salt content in gel polymer electrolyte (GPE)

The binary solution is associated with a polymer to form the GPE. The initial GPE composition is 70 wt % of liquid binary solution and 30 wt % of BEMA polymer. For the salt content  $R = 0.3$ , the integration of the binary solution in the GPE leads to a decrease of about 52 % of the ionic conductivity ( $0.489 \text{ mS cm}^{-1}$  for the GPE versus  $0.93 \text{ mS cm}^{-1}$  for the corresponding liquid binary solution). The Arrhenius plots (not shown here) exhibit a VFT behavior typical of amorphous materials.  $B$  and  $T_0$  parameters are higher than those of the binary solution are ( $7.12 \text{ kJ mol}^{-1}$  and  $190.3 \text{ }^\circ\text{C}$ ) which evidences the confinement of the liquid phase and its interactions with the polymer. NMR measurements are done at  $25 \text{ }^\circ\text{C}$  for the lower salt content while  $60 \text{ }^\circ\text{C}$  are necessary for the higher salt content ( $R = 0.6$ ) to be able to detect Li diffusion. When the salt ratio increases (Figure 7a), the diffusion coefficients of H and F decrease as expected due to the viscosity increase. This evolution is the same as the one reported in binary liquid (Figure 4a) evidencing the low interaction of the polymer network with the ionic liquid as reported by Sotta *et al* [21] for the percolating part of the liquid phase. By contrast, the diffusion coefficient of Li drastically decreases in the GPE. This drop is accentuated by the salt content increase up to 0.3. Beyond this concentration, the diffusion coefficient of Li remains quite stable while those of H and F continue to decrease. This trend is more significant on the transference numbers evolution in Figure 7b. The transference number  $T_H$  steadily decreases while the  $T_F$  increases due to the increase of TFSI<sup>-</sup> concentration with salt content. On the contrary, the Li transference number sharply decreases up to  $R = 0.3$  where it reaches a minimum before a slight increase for higher salt content. Considering the diffusion evolution of F and Li, we can assume that below  $R = 0.3$ ,

$\text{Li}^+$  are no more solvated by  $\text{TFSI}^-$  as previously observed in binary solutions (Figure 4) and  $[\text{Li}_2(\text{TFSI})_n]^{2-n}$  complexes are dissociated in the presence of BEMA. This assumption is confirmed by Raman spectra (supporting file Figure S4) showing that the only remaining band corresponds to the "free" TFSI. In the case of GPE,  $\text{Li}^+$  are complexed to PEO groups of BEMA polymer though about five oxygens forming a crown around the cation [65, 66].  $\text{Li}^+$  transport mechanism is then a mix between hopping among complexation sites assisted by polymer segmental motion. In this type of amorphous material, segmental motion is strongly dependent of the system viscosity. Hence, a salt ratio increase induces an increase of the viscosity and thus limits the motion of lithium ions. Above 0.3, the viscosity still increases but lithium diffusion is stable. It shows that beyond a critical salt concentration, the transport mechanism is more complex. We can imagine that the majority of PEO complexation sites is occupied or the steric hindrance of PEO chains does not allow more complexation of added  $\text{Li}^+$ . Hence, a part of  $\text{Li}^+$  is no more solvated by PEO chains but remains as ionic complexes in the liquid phase.  $\text{Li}^+$  ions can then move either by ionic migration among the liquid phase or by hops assisted by the PEO segmental motion. This assumption is strengthened by Raman spectra (supporting file Figure S4) where a slight shoulder around  $742\text{ cm}^{-1}$  appears for the higher salt content. This phenomenon induces a slight increase of the Li transference number for the higher salt content. However, most of Li being solvated by PEO chains, we can imagine that ionic complexes with  $\text{TFSI}^-$  will be preferentially monodendate forming  $[\text{Li}(\text{TFSI})_4]^{3-}$  with high negative charge. Galvanostatic cycling, presented in Figure 7c, shows that cycling ability is improved by increasing salt content. Cycling performance are poor for the lower salt contents ( $R < 0.2$ ) and greatly improved above  $R = 0.3$ . This concentration corresponds with the slope change on the transference number evolution as reported above (Figure 7b). According to previous results and interpretations, cycling performances can be

limited by restricted segmental motion, which limits Li transfer by hopping. When the salt content increases beyond  $R = 0.3$ , a part of the Li transport is ensured by ionic migration in the liquid phase which can explain the better cycling ability. Thus, the limiting factor appears to be the segmental motion of the polymer network. The explored strategy is to enhance segmental motion by introducing a linear polymer that decreases the crosslinking density of the polymer network.

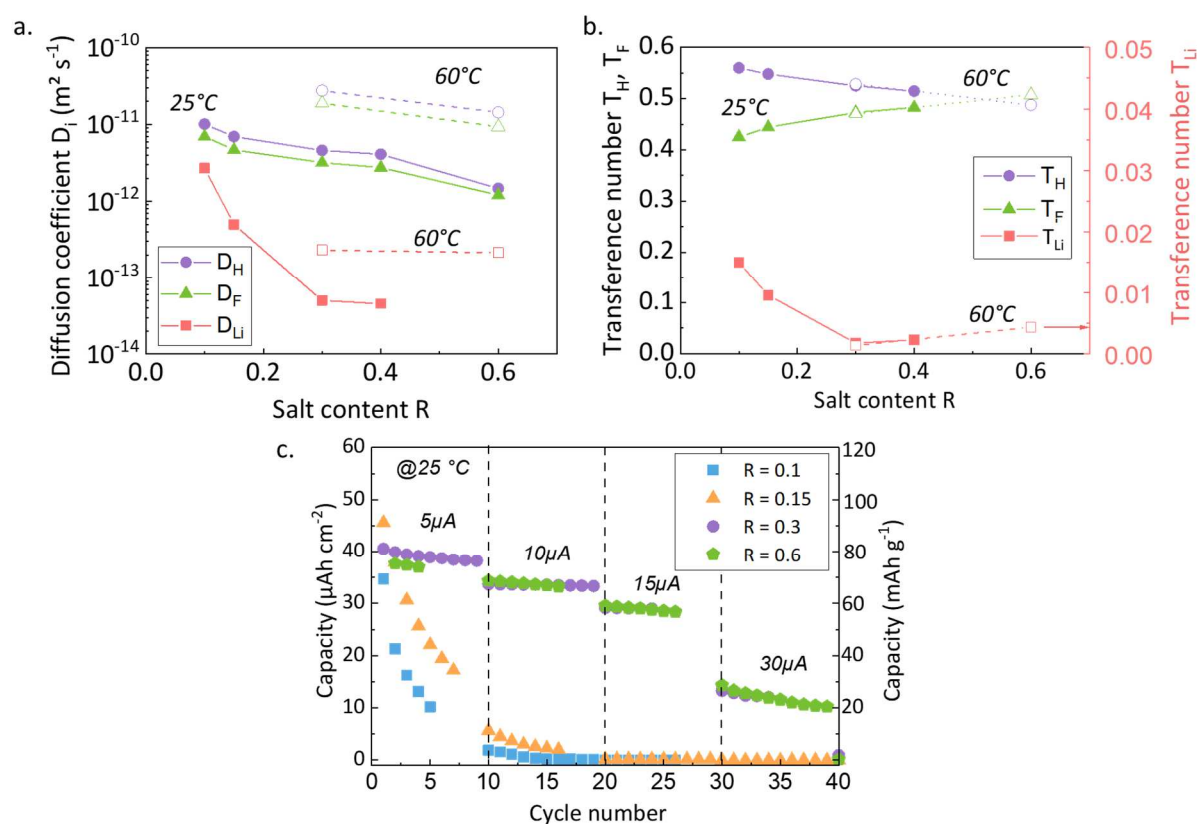


Figure 7: Evolution of the diffusion coefficients (a) and apparent transference number (b) of  $^1\text{H}$ ,  $^{19}\text{F}$  and  $^7\text{Li}$  nuclei determined by NMR measurements at  $25^\circ\text{C}$  (solid lines) and  $60^\circ\text{C}$  (dash lines); Galvanostatic cycling at various currents for GPE integrating various salt content binary solutions (c).

### 3.3 Influence of the linear polymer content

The chosen linear polymer is a monomethacrylate, the polyethylene glycol methacrylate (PEGMA). To avoid the stability limitation in reduction ( $\sim 2.5\text{V}$  vs  $\text{Li}^+/\text{Li}$ ),  $-\text{OH}$  pending functions are replaced by methoxide groups (poly(ethylene glycol) methyl ether

methacrylate (me-PEGMA)). The synthesis protocol is the same (70 wt% of liquid binary phase, 30 wt% of polymer) except that a proportion of BEMA is replaced by me-PEGMA which leads to a decrease of the ratio Li/(crosslinking points, CP). The number of crosslinking points CP is determined such as 1 mol of BEMA equals 2 mol of crosslinking points considering the two methacrylate functions and 1 mol of me-PEGMA corresponds to 1 mol of crosslinking points. Considering the previous results, the salt content is fixed at  $R = 0.6$ . The addition of linear me-PEGMA directly affects the GPE mechanical properties. The theoretical crosslinking density of the polymer can be determined by the following equation [67]:

$$v_e = \frac{E}{3RT} \text{ (eq.6)}$$

Where  $v_e$  is the crosslinking density ( $\text{mol m}^{-3}$ ),  $R$  the perfect gas constant ( $8.314 \text{ J mol}^{-1} \text{ K}^{-1}$ ) and  $T$  the temperature (K). Theoretical crosslinking density is close to the expected one, i.e.  $2 \times [\text{BEMA}]$  considering the presence of two methacrylate functions per BEMA molecule. The Young's modulus decreases linearly with  $v_e$  and thus with the BEMA concentration and me-PEGMA addition (Table 2). This lower mechanical strength comes with an increase of the ionic conductivity up to  $0.26 \text{ mS cm}^{-1}$  for the higher content ( $0.14 \text{ mS cm}^{-1}$  without me-PEGMA). This value is close to the binary liquid solution one (Table 1). The diffusion coefficients of H and F (Figure 8a) slightly increase with me-PEGMA ratios but transference numbers (not shown here) remains quite constant. The increase of chain polymer mobility enhances the diffusion in the liquid phase illustrating the interpenetrated morphology of the GPE. The Li transport, assuming to be mostly provided by hops assisted by segmental motion, doubles with me-PEGMA addition. The increase is significant with 9 wt% me-PEGMA but remains quite limited with higher me-PEGMA content. This is consistent with previous

results assuming a complex mechanism with hops assisted by segmental motion and ionic diffusion in the liquid phase. The addition of me-PEGMA increases segmental motion leading to a rise of Li diffusion. No obvious improvement is observed with higher me-PEGMA content considering that the limiting phenomenon is the viscosity of the binary solution, amplified by the high salt content  $R = 0.6$ . Considering the increase of the total ionic conductivity and the evolution of Li transference number, best cycling results are expected with the higher me-PEGMA content (15B-85P, 25.5 wt%). Galvanostatic cycling (Figure 8c) shows that polarization is lower with the addition of me-PEGMA. Discharge capacity values (Figure 8b) are quite similar for the lower current ( $< 15 \mu\text{A}$ ) but high current ability is greatly improved with me-PEGMA addition. This result is in good accordance with previous measurements that show an increase of the Li conductivity with me-PEGMA content.

Compositions	Li/CP	E	$v_e$	$2*[BEMA]$	$\sigma_{tot} (25^\circ\text{C})$
wt%	mol	MPa	$\text{mol m}^{-3}$	$\text{mol m}^{-3}$	$\text{mS cm}^{-1}$
100B-0P	2.0	3.70	498	456	0.14
70B-30P	2.9	2.84	382	317	0.20
50B-50P	4.1	2.09	281	226	0.23
30B-70P	6.8	1.21	163	135	0.25
15B-85P	13.7	0.52	70	68	0.26

Table 2: Various physico-chemical properties of GPE containing  $R = 0.6$   $\text{PYR}_{13}\text{TFSI-LiTFSI}$  binary solution at 70 wt% and 30 wt% of polymer consisting of  $X$  wt% of BEMA and  $(1-X)$  wt% of me-PEGMA. B =BEMA, P= me-PEGMA, CP = crosslinking point.

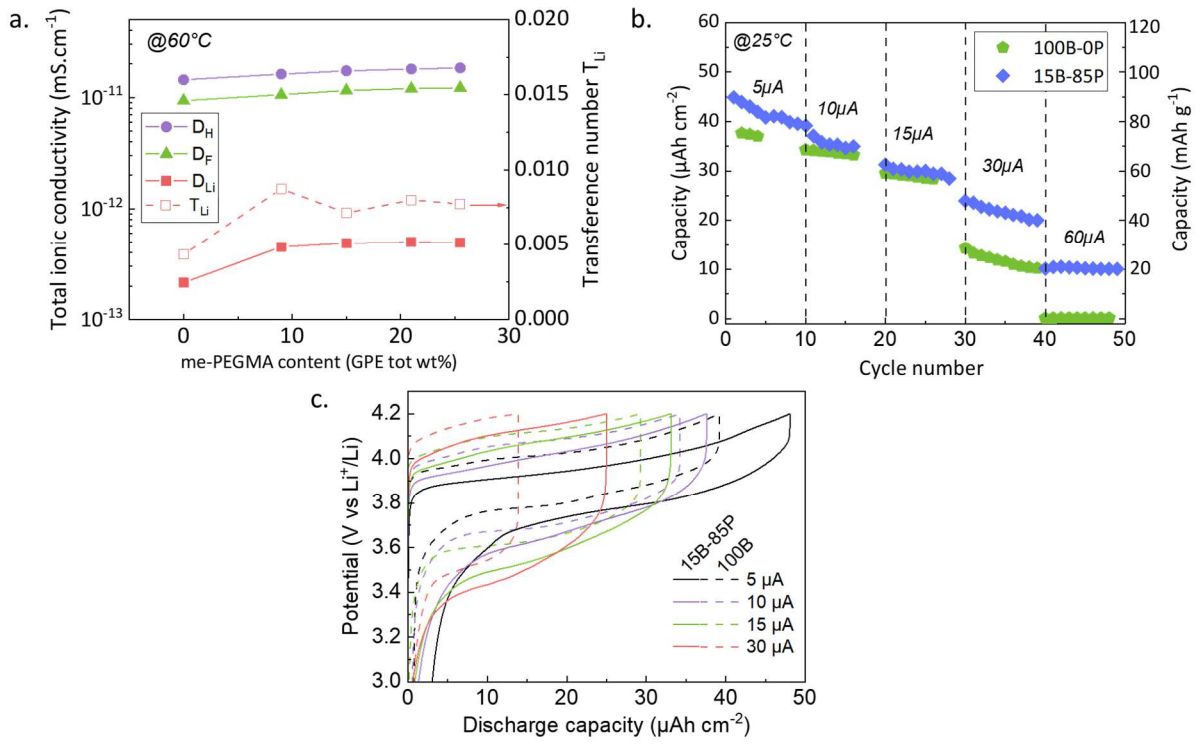


Figure 8: Evolution of the diffusion coefficients of H, F and Li and apparent transference number of Li at 60°C (a); Galvanostatic cycling of  $\text{LiCoO}_2/\text{GPE}/\text{Li}$  coin cells integrating 100 wt% BEMA or 15-85 wt% BEMA:me-PEGMA polymer for various current at 25°C (b) and corresponding cycling curves (c).

## Conclusion

Pyr<sub>13</sub>TFSI and LiTFSI are chosen for their good thermal stability fitting with new emerging applications. When the salt content increases, the total ionic conductivity severely drops (up to – 95 %) due to the large viscosity rise. NMR spectroscopy shows that apparent transference number of lithium is boosted by the salt addition with an optimum of Li conductivity around  $R = 0.3$  ( $0.08 \text{ mS cm}^{-1}$ ). The evolution of the dissociation ratio  $\Delta_{\text{NMR}}$  shows that the quantity of neutral species increases (up to 60 %) with the salt content as also predicted by the evolution of the prefactor A in VTF fittings. By combining these results with Raman spectroscopy, we can assume that for the lower salt concentration, monodentate complexes  $[\text{Li}(\text{TFSI})_4]^{3-}$  are formed. With salt addition, these complexes are converted into bidentate coordinated complexes  $[\text{Li}(\text{TFSI})_2]^-$  with a low mean negative charge. With higher salt concentration, large clusters  $(\text{Li}_2[\text{TFSI}]_y)^{z-y}$ , binding several Li together, are formed. These complexes and aggregates present mean negative charges that greatly influence cycling performances. Hence, monodentate complexes exhibit a high negative charge that seems to be detrimental for galvanostatic cycling. The increase of salt content, decreasing the mean charge of complexes involving Li, improves the cycling performances despite the ionic conductivity drop (60 % remaining discharge capacity at C). The integration of binary solution in GPE generates an additional transport mechanism by hops assisted by segmental motion due to the Li coordination by oxygen of PEO chains. When salt concentration increases,  $T_{\text{Li}}$  is enhanced by adding migration in the liquid phase to hopping transport. This leads to a great improvement of electrochemical performances above  $R = 0.3$ . The addition of linear polymer (me-PEGMA) limits mechanical properties of

the GPE but significantly improves ionic conductivity (close to the liquid one) by enhancing segmental motion. Hence, the Li transference number is multiplied by two and discharge capacity is close to 70 % of the theoretical one at 25 °C. This study showed that a deep understanding of ionic interactions can help putting forward further optimizations especially on the choice of components nature in electrolytes (acrylate functions substitution, cation choice, etc.).

### **Acknowledgements**

The authors thank P.A. Bayle (Univ. Grenoble Alpes, CEA, INAC-MEM, LRM, MINATEC Campus) for helpful discussions and technical expertise on PFG-NMR measurements.

This study was founded through the EnSO European project. EnSO has been accepted for funding within the Electronic Components and Systems For European Leadership Joint Undertaking in collaboration with the European Union's H2020 Framework Program (H2020/2014-2020) and National Authorities, under grant agreement n° 692482.

## References

- [1] J.B. Goodenough and Y. Kim, *Chem. Mater.*, 22 (2010) 587.
- [2] S.F. Zopf, A.J. D'Angelo, H. Qin and M.J. Panzer, *CHAPTER 14 Wearable Energy Storage Based on Ionic Liquid Gels*, in *Polymerized Ionic Liquids*. 2018, The Royal Society of Chemistry. 381.
- [3] M.V.M. Reddy, A.; Julien, C.M.; Paoella, A.; Zaghbi, K., *Materials*, 13 (2020) 1884.
- [4] M. Armand, *Solid State Ionics*, 69 (1994) 309.
- [5] F. Zheng, M. Kotobuki, S. Song, M.O. Lai and L. Lu, *J. Power Sources*, 389 (2018) 198.
- [6] S. Liang, W. Yan, X. Wu, Y. Zhang, Y. Zhu, H. Wang and Y. Wu, *Solid State Ionics*, 318 (2018) 2.
- [7] X. Cheng, J. Pan, Y. Zhao, M. Liao and H. Peng, *Adv. Energy Mater.*, 8 (2018)
- [8] S. Chen, K. Wen, J. Fan, Y. Bando and D. Golberg, *Journal of Materials Chemistry A*, 6 (2018) 11631.
- [9] J. Kalhoff, G.G. Eshetu, D. Bresser and S. Passerini, *ChemSusChem*, 8 (2015) 2154.
- [10] G. Feuilleade and P. Perche, *J. Appl. Electrochem.*, 5 (1975) 63.
- [11] J.M. Tarascon, A.S. Gozdz, C. Schmutz, F. Shokoohi and P.C. Warren, *Solid State Ionics*, 86-88 (1996) 49.
- [12] A. Noda and M. Watanabe, *Electrochim. Acta*, 45 (2000) 1265.
- [13] P. Yang, L. Liu, L. Li, J. Hou, Y. Xu, X. Ren, M. An and N. Li, *Electrochim. Acta*, 115 (2014) 454.
- [14] A. Farnicola, F.C. Weise, S.G. Greenbaum, J. Kagimoto, B. Scrosati and A. Soletto, *J. Electrochem. Soc.*, 156 (2009) A514.
- [15] A. Mauger, C.M. Julien, A. Paoella, M. Armand and K. Zaghbi, *Materials Science and Engineering: R: Reports*, 134 (2018) 1.
- [16] Q.-D.W. Wei Yang, Yu Lei, Zi-Pei Wan, Lei Qin, Wei Yu, Ru-Liang Liu, Deng-Yun Zhai, Hong Li, Bao-Hua Li, Fei-Yu Kang, *Chin. Phys. B*, 27 (2018) 068201.
- [17] M. Moreno, E. Simonetti, G.B. Appetecchi, M. Carewska, M. Montanino, G.-T. Kim, N. Loeffler and S. Passerini, *J. Electrochem. Soc.*, 164 (2017) A6026.
- [18] H. Zhang, W. Qu, N. Chen, Y. Huang, L. Li, F. Wu and R. Chen, *Electrochim. Acta*, 285 (2018) 78.
- [19] X.-B. Cheng, R. Zhang, C.-Z. Zhao and Q. Zhang, *Chem. Rev.*, 117 (2017) 10403.
- [20] J.R. Nair, L. Porcarelli, F. Bella and C. Gerbaldi, *ACS Appl. Mater. Interfaces*, 7 (2015) 12961.

- [21] D. Sotta, J. Bernard and V. Sauvant-Moynot, *Prog. Org. Coat.*, 69 (2010) 207.
- [22] J. Rymarczyk, M. Carewska, G.B. Appetecchi, D. Zane, F. Alessandrini and S. Passerini, *Eur. Polym. J.*, 44 (2008) 2153.
- [23] B. Rupp, M. Schmuck, A. Balducci, M. Winter and W. Kern, *Eur. Polym. J.*, 44 (2008) 2986.
- [24] J.R. Nair, F. Colò, A. Kazzazi, M. Moreno, D. Bresser, R. Lin, F. Bella, G. Meligrana, S. Fantini, E. Simonetti, G.B. Appetecchi, S. Passerini and C. Gerbaldi, *J. Power Sources*, 412 (2019) 398.
- [25] M.-K. Song, J.-Y. Cho, B.W. Cho and H.-W. Rhee, *J. Power Sources*, 110 (2002) 209.
- [26] J.R. Nair, C. Gerbaldi, G. Meligrana, R. Bongiovanni, S. Bodoardo, N. Penazzi, P.Reale and V. Gentili, *J. Power Sources*, 178 (2008) 751.
- [27] C. Gerbaldi, J.R. Nair, G. Meligrana, R. Bongiovanni, S. Bodoardo and N. Penazzi, *J. Appl. Electrochem.*, 39 (2009) 2199.
- [28] C. Gerbaldi, J.R. Nair, S. Ahmad, G. Meligrana, R. Bongiovanni, S. Bodoardo and N. Penazzi, *J. Power Sources*, 195 (2010) 1706.
- [29] A. Chiappone, J.R. Nair, C. Gerbaldi, R. Bongiovanni and E. Zeno, *Electrochim. Acta*, 153 (2015) 97.
- [30] W. Fan, N.-W. Li, X. Zhang, S. Zhao, R. Cao, Y. Yin, Y. Xing, J. Wang, Y.-G. Guo and C. Li, *Advanced Science*, 5 (2018) 1800559.
- [31] H. Porthault, G. Piana, M. Cesbron, V. Armel, A. Bazin, S. Franger and S. Oukassi, *J. Phys. Chem. C*, 123 (2019) 18171.
- [32] P.G. Bruce, J. Evans and C.A. Vincent, *Solid State Ionics*, 28-30 (1988) 918.
- [33] K.M. Diederichsen, E.J. McShane and B.D. McCloskey, *ACS Energy Letters*, 2 (2017) 2563.
- [34] M. Watanabe, S. Nagano, K. Sanui and N. Ogata, *Solid State Ionics*, 28-30 (1988) 911.
- [35] M.M. Hiller, M. Joost, H.J. Gores, S. Passerini and H.D. Wiemhöfer, *Electrochim. Acta*, 114 (2013) 21.
- [36] A. Chiappone, S. Jeremias, R. Bongiovanni and M. Schönhoff, *J. Polym. Sci., Part B: Polym. Phys.*, 51 (2013) 1571.
- [37] I. Rey, P. Johansson, J. Lindgren, J.C. Lassègues, J. Grondin and L. Servant, *The Journal of Physical Chemistry A*, 102 (1998) 3249.
- [38] W. Lee, S. Muhammad, C. Sergey, H. Lee, J. Yoon, Y.-M. Kang and W.-S. Yoon, *Angew. Chem. Int. Ed.*, 59 (2020) 2578.
- [39] K. Mizushima, P.C. Jones, P.J. Wiseman and J.B. Goodenough, *Mater. Res. Bull.*, 15 (1980) 783.

- [40] M. Kunze, S. Jeong, E. Paillard, M. Winter and S. Passerini, *The Journal of Physical Chemistry C*, 114 (2010) 12364.
- [41] I. Nicotera, C. Oliviero, W.A. Henderson, G.B. Appetecchi and S. Passerini, *The Journal of Physical Chemistry B*, 109 (2005) 22814.
- [42] D.R. MacFarlane, M. Forsyth, E.I. Izgorodina, A.P. Abbott, G. Annat and K. Fraser, *PCCP*, 11 (2009) 4962.
- [43] G.A. Giffin, A. Moretti, S. Jeong, K. Pilar, M. Brinkkötter, S.G. Greenbaum, M. Schönhoff and S. Passerini, *ChemSusChem*, 11 (2018) 1981.
- [44] J. Mindemark, M.J. Lacey, T. Bowden and D. Brandell, *Prog. Polym. Sci.*, 81 (2018) 114.
- [45] K.M. Diederichsen, H.G. Buss and B.D. McCloskey, *Macromolecules*, 50 (2017) 3831.
- [46] P. Sippel, P. Lunkenheimer, S. Krohns, E. Thoms and A. Loidl, *Sci. Rep.*, 5 (2015) 13922.
- [47] C.A. Angell, *J. Res. Nat. Inst. Stand. Technol.*, 102 (1997) 171.
- [48] M. Galiński, A. Lewandowski and I. Stępnia, *Electrochim. Acta*, 51 (2006) 5567.
- [49] D. Bresser, S. Lyonnard, C. Iojoiu, L. Picard and S. Passerini, *Molecular Systems Design & Engineering*, (2019)
- [50] D.R. MacFarlane, P. Meakin, J. Sun, N. Amini and M. Forsyth, *The Journal of Physical Chemistry B*, 103 (1999) 4164.
- [51] C.S. Stefan, D. Lemordant, P. Biensan, C. Siret and B. Claude-Montigny, *J. Therm. Anal. Calorim.*, 102 (2010) 685.
- [52] H. Jin, B. O'Hare, J. Dong, S. Arzhantsev, G.A. Baker, J.F. Wishart, A.J. Benesi and M. Maroncelli, *The Journal of Physical Chemistry B*, 112 (2008) 81.
- [53] S.A. Mirkhani, F. Gharagheizi, P. Ilani-Kashkouli and N. Farahani, *Thermochim. Acta*, 543 (2012) 88.
- [54] A. Martinelli, A. Matic, P. Jacobsson, L. Börjesson, A. Fernicola and B. Scrosati, *The Journal of Physical Chemistry B*, 113 (2009) 11247.
- [55] T. Frömling, M. Kunze, M. Schönhoff, J. Sundermeyer and B. Roling, *The Journal of Physical Chemistry B*, 112 (2008) 12985.
- [56] M. Joost, M. Kunze, S. Jeong, M. Schönhoff, M. Winter and S. Passerini, *Electrochim. Acta*, 86 (2012) 330.
- [57] T. Watkins and D.A. Buttry, *The Journal of Physical Chemistry B*, 119 (2015) 7003.
- [58] J. Pitawala, A. Martinelli, P. Johansson, P. Jacobsson and A. Matic, *J. Non-Cryst. Solids*, 407 (2015) 318.

- [59] J.-C. Lassègues, J. Grondin, C. Aupetit and P. Johansson, *The Journal of Physical Chemistry A*, 113 (2009) 305.
- [60] J.L. Allen, O. Borodin, D.M. Seo and W.A. Henderson, *J. Power Sources*, 267 (2014) 821.
- [61] O. Borodin, G.D. Smith and W. Henderson, *The Journal of Physical Chemistry B*, 110 (2006) 16879.
- [62] M. Kunze, S. Jeong, E. Paillard, M. Schönhoff, M. Winter and S. Passerini, *Adv. Energy Mater.*, 1 (2011) 274.
- [63] S. Duluard, J. Grondin, J.-L. Bruneel, I. Pianet, A. Grélard, G. Campet, M.-H. Delville and J.-C. Lassègues, *J. Raman Spectrosc.*, 39 (2008) 627.
- [64] J. Wang, Y. Yamada, K. Sodeyama, C.H. Chiang, Y. Tateyama and A. Yamada, *Nature Communications*, 7 (2016) 12032.
- [65] W.H. Meyer, *Adv. Mater.*, 10 (1998) 439.
- [66] P.G. Bruce, *Dalton Trans.*, (2006) 1365.
- [67] J.-P. Pascault, H. Sautereau, J. Verdu and R.J.J. Williams, *Thermosetting Polymers*. 2002: Marcel Dekker.

Graphical Abstract

